

# Crystal structure of the catalytic D2 domain of the AAA+ ATPase p97 reveals a putative helical split-washer-type mechanism for substrate unfolding

Lasse Stach<sup>1</sup>, Rhodri Marc Morgan<sup>2</sup> , Linda Makhoulouf<sup>1</sup>, Alice Douangamath<sup>3</sup>, Frank von Delft<sup>3,4,5</sup>, Xiaodong Zhang<sup>1</sup>  and Paul S. Freemont<sup>1</sup> 

- 1 Section of Structural and Synthetic Biology, Department of Infectious Disease, Imperial College London, UK
- 2 Centre for Structural Biology, Department of Life Sciences, Imperial College London, UK
- 3 Diamond Light Source Ltd, Harwell Science and Innovation Campus, Didcot, UK
- 4 Structural Genomics Consortium, Nuffield Department of Medicine, University of Oxford, UK
- 5 Department of Biochemistry, University of Johannesburg, Auckland Park, South Africa

## Correspondence

P. S. Freemont, Section of Structural and Synthetic Biology, Department of Infectious Disease, Imperial College London, London SW7 2AZ, UK  
Tel: +44 (0) 207 594 5327  
E-mail: p.freemont@imperial.ac.uk

(Received 11 June 2019, revised 29 September 2019, accepted 31 October 2019, available online 22 November 2019)

doi:10.1002/1873-3468.13667

Edited by Stuart Ferguson

Several pathologies have been associated with the AAA+ ATPase p97, an enzyme essential to protein homeostasis. Heterozygous polymorphisms in p97 have been shown to cause neurological disease, while elevated proteotoxic stress in tumours has made p97 an attractive cancer chemotherapy target. The cellular processes reliant on p97 are well described. High-resolution structural models of its catalytic D2 domain, however, have proved elusive, as has the mechanism by which p97 converts the energy from ATP hydrolysis into mechanical force to unfold protein substrates. Here, we describe the high-resolution structure of the p97 D2 ATPase domain. This crystal system constitutes a valuable tool for p97 inhibitor development and identifies a potentially druggable pocket in the D2 domain. In addition, its P<sub>61</sub> symmetry suggests a mechanism for substrate unfolding by p97.

## Database

The atomic coordinates and structure factors have been deposited in the PDB database under the accession numbers 6G2V, 6G2W, 6G2X, 6G2Y, 6G2Z and 6G30.

**Keywords:** AAA + ATPase; D2 domain; IBMPFD; p97

The AAA+ ATPase p97 (valosin-containing protein VCP) is a highly abundant enzyme with essential roles in multiple cellular processes [1]. It was initially identified as an Mg<sup>2+</sup>-ATPase with sixfold symmetry and an apparent molecular weight of 97 kDa, homologous to yeast cell division protein cdc48 [2,3]. The enzyme was subsequently shown to play a role in various cellular processes, both nuclear and cytoplasmic, reviewed by Meyer and Wehl [4]. These include membrane

fusion during Golgi reassembly [5], endoplasmic reticulum-associated degradation [6], NF- $\kappa$ B activation [7] and the extraction of DNA-interacting proteins from chromatin [8,9].

p97 is also associated with inclusion body myopathy with early-onset Paget disease and frontotemporal dementia (IBMPFD), an autosomal-dominant multisystem disease [10]. A set of mutations in p97 has been shown to cause this disease, which is

## Abbreviations

FL, full-length; IBMPFD, inclusion body myopathy with early-onset Paget disease and frontotemporal dementia; ITC, isothermal titration calorimetry; VAT, VCP-like ATPase.

marked by muscle weakness, early-onset Paget disease and frontotemporal dementia on the physiological level, and unregulated, excessive enzymatic activity at the molecular level [10]. Inhibition of p97 has also been shown to be an effective method of provoking proteotoxic stress in cancer chemotherapy [11].

Each p97 protomer consists of a noncatalytic N-terminal and two ATPase domains D1 and D2. Both crystallographic and cryo-electron microscopy studies have shown that in the physiological hexamer, the ATPase domains form planar rings with sixfold symmetry with the N domain either coplanar to the D1 domain or sitting 'on top' of the protein [12,13]. The most pronounced movement within p97 has been reported for the N domains. Depending on whether ADP or ATP is bound to the protein, these domains have been observed in a D1 coplanar state (ADP bound) or in an 'up' position (ATP bound) [12]. The N domain makes interactions with p97 cofactors, which allow p97 to mediate diverse physiological roles [14]. These proteins include Fas-associated factor Faf1 and the Ufd1/Npl4 heterodimer, which play a role in ERAD, and the protein p47, essential to membrane fusion [5,6,15,16]. A large proportion of p97 cofactors, including the three mentioned above, bind ubiquitin and link the ATPase p97 with the ubiquitin system, reviewed by Hanzelmann & Schindelin [17]; Stach & Freemont [1].

Both mammalian p97 and its *Saccharomyces cerevisiae* homologue cdc48 unfold proteins in a process that requires ATP hydrolysis, the presence of the Ufd1/Npl4 cofactor and a K48-linked polyubiquitinated substrate [18,19]. The substrate is unfolded by threading it through the central pore formed by the hexamer [19]. Whether the six protomers act in a processive or concerted manner, the nature of the catalytic cycle of this enzyme is less clear than the fate of its substrate. High-resolution cryo-EM structures in both ADP- and ATP-bound states were shown to be symmetric, supporting a concerted mechanism [12]. On the other hand, it has been shown that the D2 ring can only bind 3 or 4 molecules of ATP $\gamma$ S, suggesting an asymmetry in the p97 hexamer and a processive enzyme mechanism [20]. In addition, analysis of the p97 structures submitted to the PDB has identified asymmetry in a number of depositions, significantly in those that contain the D1-D2 linker region that has been proposed to induce asymmetry [21].

The mechanism by which p97 converts the energy of ATP hydrolysis into mechanical force to unfold

proteins has also not yet been determined, but there is evidence of a split-washer-type mechanism for its archaeal homologue VCP-like ATPase (VAT) [22]. In its ATP-bound state, the ATPase domains form planar rings, but in the ADP-bound state, the 12 ATPase domains form a continuous, helical, split-washer conformation [22]. It has been proposed that the conformational changes from planar to helical conformation provide the mechanical energy for unfolding. Interestingly, there is considerable conservation between p97 and VAT, in terms of both sequence and function. Pairwise structure comparison reveals 53% sequence identity over 254 aligned residues of p97 D2 domain compared to VAT ( $z$ -score 25.9 and rmsd of 2.3) (DALI server, [23]). The archaeal protein unfolds substrates tagged with the C-terminal degradation tag *ssrA* [24]. While wild-type p97 is not active against such substrates, a p97 construct with two-point mutants in the D1 pore and an N domain deletion effectively unfolds *ssrA* substrates, suggesting these two ATPases are related mechanistically [25]. Furthermore, VAT has been shown to unfold substrates by threading them through the central pore, as also reported for *cdc48* [19,26]. Similarly, the disaggregase Hsp104, found in lower eukaryotes, threads its substrates through the central pore in a ratchet-like mechanism [27].

The majority of drug discovery efforts developing p97 inhibitors focus on the D2 domain as it mediates the main catalytic activity. The ATP-competitive inhibitor CB-5083 is specific for the D2 active sites, while the well-characterised allosteric inhibitor NMS-873 interacts with a region spanning the D1 and D2 domains of adjacent protomers [28,29]. Structural information about the D2 domain, however, which may aid such efforts, is limited to low-resolution crystal structures in a nonphysiological heptamer, with mutations and deletions in D2 or low-throughput cryo-EM [12,30,31].

Here, we report the crystal structure of the minimal p97 D2 domain crystallised in a P6<sub>1</sub> space group closely resembling the VAT helical conformation, suggesting the split-washer-type mechanism may be conserved from archaea to metazoans. This crystal system also has potential as a tool for developing novel inhibitors against the p97 D2 ATPase domain, and we describe a fragment-based screen to identify potential novel p97 chemical ligands. The recent termination of all CB-5083 clinical trials due to off-target effects [32] highlights the need to develop novel inhibitors against this promising drug target (ClinicalTrials.gov Identifiers NCT02243917 and NCT02223598).

## Materials and methods

### Molecular biology, protein expression and purification

Fragments of the human p97 gene, coding for the FL protein (amino acids 1-806), a C-terminal truncation (1-764), ND1 (1-481), D2 domain (463-764) and the D2 with a C-terminal extension (463-806), were amplified by PCR and cloned into the pET47b vector (Novagen/Merck, Darmstadt, Germany). The resultant constructs with N-terminal polyhistidine tags were expressed in *E. coli* BL21 DE3 gold cells (Agilent, Santa Clara, CA, USA) grown in LB. Cultures were induced at OD<sub>600</sub> of 0.6 at 20 degrees and grown overnight. Cell pellets were suspended in 500 mM NaCl, 50 mM Tris pH8.0, 0.5 mM TCEP and 10 mM imidazole. Clarified cell lysate was purified by Ni-affinity followed by size-exclusion chromatography using a KW804 gel filtration column (Shodex, Tokyo, Japan). Gel filtration buffer was 150 mM NaCl, 20 mM Tris pH7.5 and 0.5 mM TCEP. For protein used in crystallisation, the polyhistidine tag was removed prior to gel filtration using rhinovirus 3C protease. The protease was used at a molar ratio of 1/500 at 4 degrees overnight and not specifically removed as it was used at such a low ratio.

### Protein crystallisation

Crystallisation drops were set up at room temperature in MRC 2-well plates (Swissci, Neuheim, Switzerland) using a Mosquito robot (TTP Labtech, Melbourn, UK) using 100 nL of 8 mg·mL<sup>-1</sup> p97 D2 in gel filtration buffer and 100 nL of well solution. Initial crystals grew in: 0.12 M 1,6-hexanediol; 0.12 M 1-butanol; 0.12 M 1,2-propanediol; 0.12 M 2-propanol; 0.12 M 1,4-butanediol; 0.12 M 1,3-propanediol; 0.1 M sodium HEPES; 0.1 M MOPS; 12.5% v/v MPD; 12.5% poly(ethylene glycol) 1000; and 12.5% w/v poly(ethylene glycol) 3350 at pH 7.5 (Molecular Dimensions Morpheus D4). Crystals were used to produce a microseed solution using a Seed Bead (Hampton Research) according to the manufacturer's instructions. Optimised crystals were grown in EasyXtal (Qiagen, Hilden, Germany) 15-well plates (Qiagen) from drops containing 1 µL protein solution, 500 nL microseed solution and 1 µL of 0.08 M L-Na-glutamate; 0.08 M alanine (racemic); 0.08 M glycine; 0.08 M lysine HCl (racemic); 0.08 M serine (racemic), 0.08 M Tris, 0.08 M Bicine, 10% v/v MPD; 10% poly(ethylene glycol) 1000; 10% w/v poly(ethylene glycol) 3350 at pH 8.5 (Molecular Dimensions Morpheus H12 diluted with water to 80%). Crystal soaking as part of the XChem experiment was performed according to Collins *et al.* [33]. Crystals were soaked for 1 h in 50 mM screening compound at a final DMSO concentration of 10% in the crystal drop before flash-freezing in liquid nitrogen.

### Crystallography

Crystals were flash-frozen in liquid nitrogen, and diffraction data were collected at Diamond Light Source beamlines IO3 and I04-1. Diffraction images were indexed, scaled and integrated using XDS [34]. The data set was phased by molecular replacement using part of the structure of 5FTJ and the program phaser [35]. The structure was refined using phenix.refine and manual model building using coot [35,36]. Structural information was visualised using PyMOL (The PyMOL Molecular Graphics System, version 1.8; Schrödinger, LLC, New York, NY, USA) and UCSF chimera [37].

### ATPase assay

The ATPase assay was performed using fluorescently labelled ParM on a Clariostar plate reader (BMG) measuring at 540 nm excitation and 585 nm emission. The ParM was prepared and applied in the ATPase assay as described in Kunzelmann and Webb [38]. Enzyme concentration was 100 nM with substrate concentrations as indicated. Measurements were made every 2 min, and the increase in fluorescence fitted to a linear regression. Michaelis–Menten kinetics were calculated using PRISM 7 (GraphPad, San Diego, CA, USA). For the experiments testing sensitivity of p97 constructs to inhibitors CB-5083 and NMS-873, 250 µM ATP and 100 µM inhibitor were used.

### Multiangle laser light scattering

Samples of purified protein were applied at a flow rate of 0.5 mL·min<sup>-1</sup> to a KW804 column (Shodex) pre-equilibrated in 150 mM NaCl, 20 mM Tris/HCl pH 8.0 and 0.5 mM TCEP and mounted on an Infinity Isocratic Pump (Agilent). A DAWN-TREOS multiangle laser light scattering detector (Wyatt Technology Corp., Santa Barbara, CA, USA) recorded the scattered light intensity of the column eluent at 3 angles. The protein concentration of the eluent was determined from the change in the refractive index (dn/dc = 0.186) detected by an Optilab rEX differential refractometer equipped with a Peltier temperature-regulated flow cell, maintained at 25 °C (Wyatt Technology Corp.). The weight-averaged molecular weight of material contained in the chromatographic peaks was determined with ASTRA (Wyatt Technology Corp.).

### Isothermal titration calorimetry

Isothermal titration calorimetry experiments were performed using an ITC-200 microcalorimeter (MicroCal/Malvern Panalytical, Malvern, UK) and analysed using ORIGIN software as per the manufacturer's instructions assuming a single-site binding model. Proteins were dialysed into 150 mM NaCl, 20 mM Tris/HCl pH 8.0, 0.5 mM

TCEP and 2% DMSO, and their concentrations were determined using UV/visible spectrophotometry. Small molecules were weighed out and dissolved in the same buffer as the protein. All titrations were performed at 20 °C using 19 injections of 2  $\mu$ L each.

## Results

### Enzyme kinetics of p97 deletion mutants

In order to obtain a p97 construct containing the D2 domain in its physiological hexameric state, we carried out a p97 deletion analysis. We generated constructs of the full-length protein (FL), of a C-terminal deletion ( $\Delta$ C), of the N domain, the D1 domain and the D1-D2 linker (ND1L), of the D2 domain with

surrounding linker regions (D2L) and of the D2 domain with the D1-D2 linker (D2S) of p97 that were expressed recombinantly in *Escherichia coli* and purified (Fig. 1A).

The ATPase activity of the proteins was measured, and all five display some degree of activity (Figs 1B and S1). The FL,  $\Delta$ C and ND1L constructs have activity that fits well with a Michaelis–Menten model and is consistent with previously reported figures [39,21]. The D2L and D2S constructs possess only a fraction of the catalytic activity. Nonetheless, all five proteins, including the newly designed D2 constructs, are catalytically active and thus likely properly folded. While the FL and  $\Delta$ C have  $K_{MS}$  of approximately 25  $\mu$ M ATP, the constructs containing only one ATPase domain have considerably lower  $K_{MS}$ ,

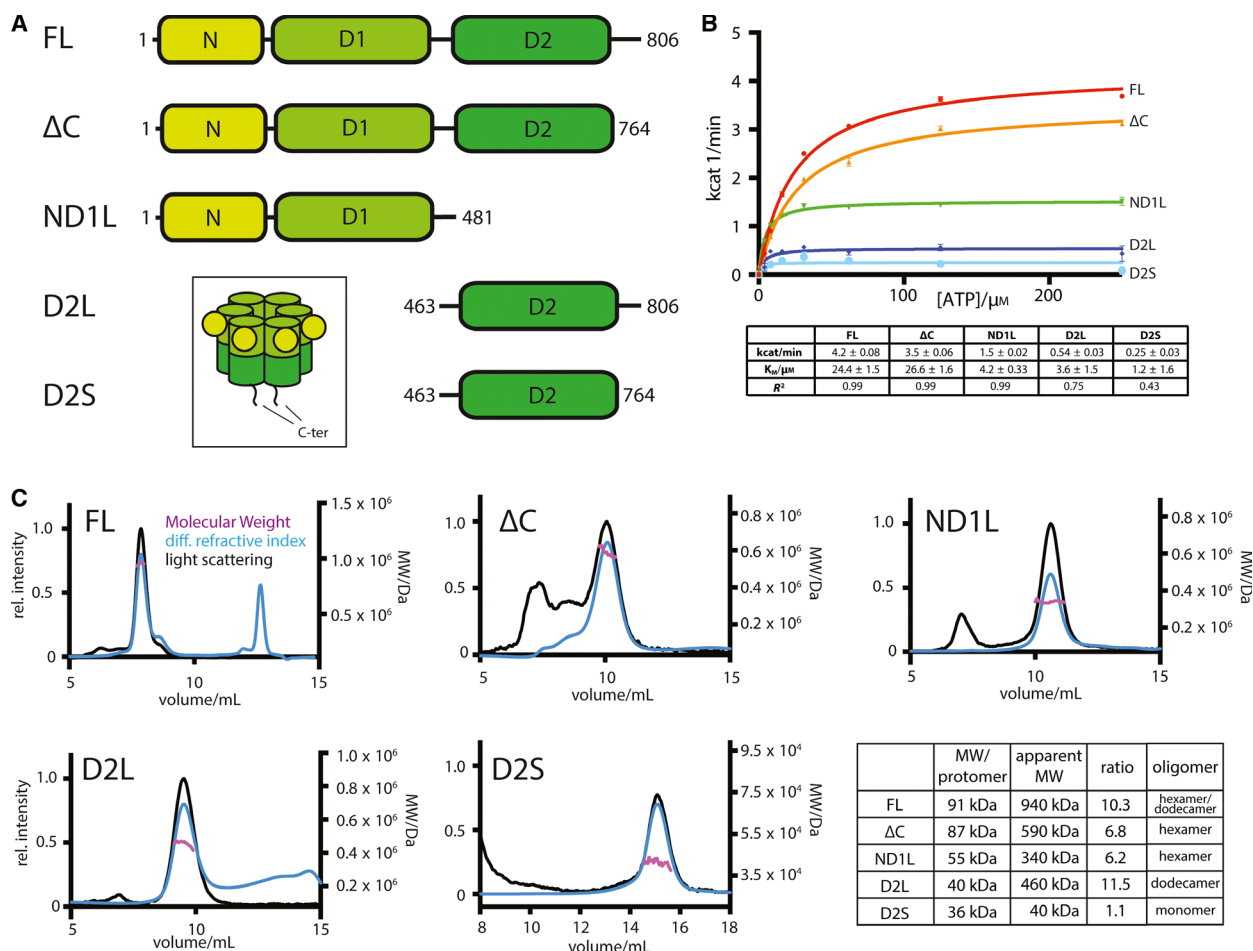


**Fig. 1.** (A) Domain organisation and boundaries of expression constructs used in this study, colour coded according to domain chartreuse: N domain, light green; D1 ATPase domain, dark green; D2 ATPase domain. Inset: schematic of p97 structure. (B) Top: Michaelis–Menten plot of ATPase activity of different p97 constructs used. Below: table with fitted parameters of Michaelis–Menten fits. (C) SEC-MALLS chromatograms showing light scattering (black), differential refractive index (blue) and fitted molecular weight (purple). The excluded volume of the KW804 column is 6 mL. Below: table comparing calculated protomer molecular weight and observed molecular weight in solution (including standard errors;  $n = 3$  technical repeats; Fig. S1) plus most likely oligomeric state of p97 constructs.

suggesting two intact ATPase rings are a prerequisite for the correct regulation of ATPase activity.

The integrity of the five proteins was also assessed, and their oligomeric states were determined using SEC-MALLS to identify constructs promising for crystallisation (Fig. 1C). These data suggest an important role for the C-terminal extension of p97 for oligomerisation of the enzyme. The FL protein has an apparent molecular weight of 940 kDa, more than 10 times larger than the 91 kDa protomer. Given that p97 is known to form highly stable hexameric rings [13], this suggests p97 FL exists in a hexamer/dodecamer equilibrium in solution. It is also unlikely that the hexamers and dodecamers can be resolved separately on the chosen size-exclusion column, hence why only one peak is visible despite the two oligomeric species present. The  $\Delta C$  construct elutes later, and its light scattering indicates a molecular weight of 590 kDa, corresponding to a hexamer. Similarly, ND1L constructs also form hexamers. The effect of the C-terminal extension is particularly clear for the two D2 constructs. The longer construct, which includes the extensions, has an apparent molecular weight of 460 kDa, corresponding to a dodecamer, while the shorter construct is monomeric.

The sensitivity of the different constructs to two known p97 inhibitors was also measured to ascertain whether these constructs could be used to determine p97 inhibitor complexes (Fig. 2A). As previously reported, the FL protein is efficiently inhibited both by the ATP-competitive inhibitor CB-5083 and the allosteric inhibitor NMS-873. The ND1L construct conversely is insensitive to either inhibitor. As expected, the D2L and D2S are sensitive to both inhibitors.

The binding of the different p97 constructs to the allosteric inhibitor NMS-873 was measured by isothermal titration calorimetry (ITC). The FL protein binds NMS-873 with a  $K_D$  of 250 nM, while the affinity of the D2S construct is approximately 10-fold weaker (Fig. 2B). As expected for an inhibitor specific for the p97 D2 domain, NMS-873 does not bind the ND1L construct. Given that D2S shows ATPase activity, remains monomeric in solution, and displays some sensitivity to both a D2-specific allosteric inhibitor and ATP-competitive one, crystallisation efforts were focused on this construct.

### Crystal structure of p97 D2S shows a helical arrangement

To this end, single well-diffracting crystals of D2S protein were obtained, and diffraction data were collected and processed up to 1.9 Å (Table S1). The crystal was in the  $P6_1$  space group, with one ATPase domain bound to ADP per asymmetric unit (Fig. 2C). In

addition, each protein molecule was also bound to a single molecule of DMSO and four molecules of MPD from the crystallisation solution. The D2 pore loop could not be resolved and is most likely disordered. The arrangement of molecules along the  $6_1$  screw axis (Fig. 2D) somewhat resembles the physiological p97 hexamer. Looking down the screw axis, the arrangement of the symmetry mates is highly similar to the arrangement of the D2 domains in the physiological hexamer when viewed from 'below' (Fig. 2E).

This similarity opens up the question as to whether this helical arrangement is purely a crystallisation artefact or of physiological significance. The interprotomer contacts of p97 in this helical conformation were compared to the structures of p97 in a planar conformation, in complex with both ADP (PDB: 5FTK) and ATP $\gamma$ S (PDB: 5FTN). Residue E587, part of the glutamate switch of p97, an important regulatory element present in AAA+ proteins, forms a salt bridge with R630 (ATP $\gamma$ S form) or R635 (ADP planar form) in the planar form (Fig. 2F)[40]. The arginine residues are part of the same loop. However, in the helical form, one protomer is moved upwards and these two arginine residues make no interprotomer contacts. Instead, N602 forms an interaction with E587 of the neighbouring protomer. While some interactions are broken in the switch to the helical conformation, new ones are formed.

### Fragment-based screening using crystals of D2S

The crystal system presented here was used for crystal-based fragment screening. As the active site of D2S in the crystal is occupied by ADP, and removal of ADP from D2S leads to protein precipitation (data not shown), the aim of the drug screening was to identify compounds that bind D2S away from the active site. These may be developed into allosteric inhibitors, possibly specific for the split-washer conformation rather than the common and prevalent ATPase active site. Including 40 control DMSO soaks, a total of 527 crystals were used in a crystallographic fragment soaking experiment conducted at the Diamond Light Source XChem facility, and data were collected from 487 crystals. Due to batch to batch variation between protein preparations and difficulties in growing well-diffracting crystals in plates compatible with the highly automated XChem set-up, only 58 crystals diffracted to better than 3.0 Å. In addition, crystal-to-crystal variability in cell dimensions and in the conformation of some surface loops made analysis of the crystals using a pan-crystal approach (PANDDA) challenging [41].

The data sets were analysed using PANDDA software, and two hits were found in the same p97 pocket.

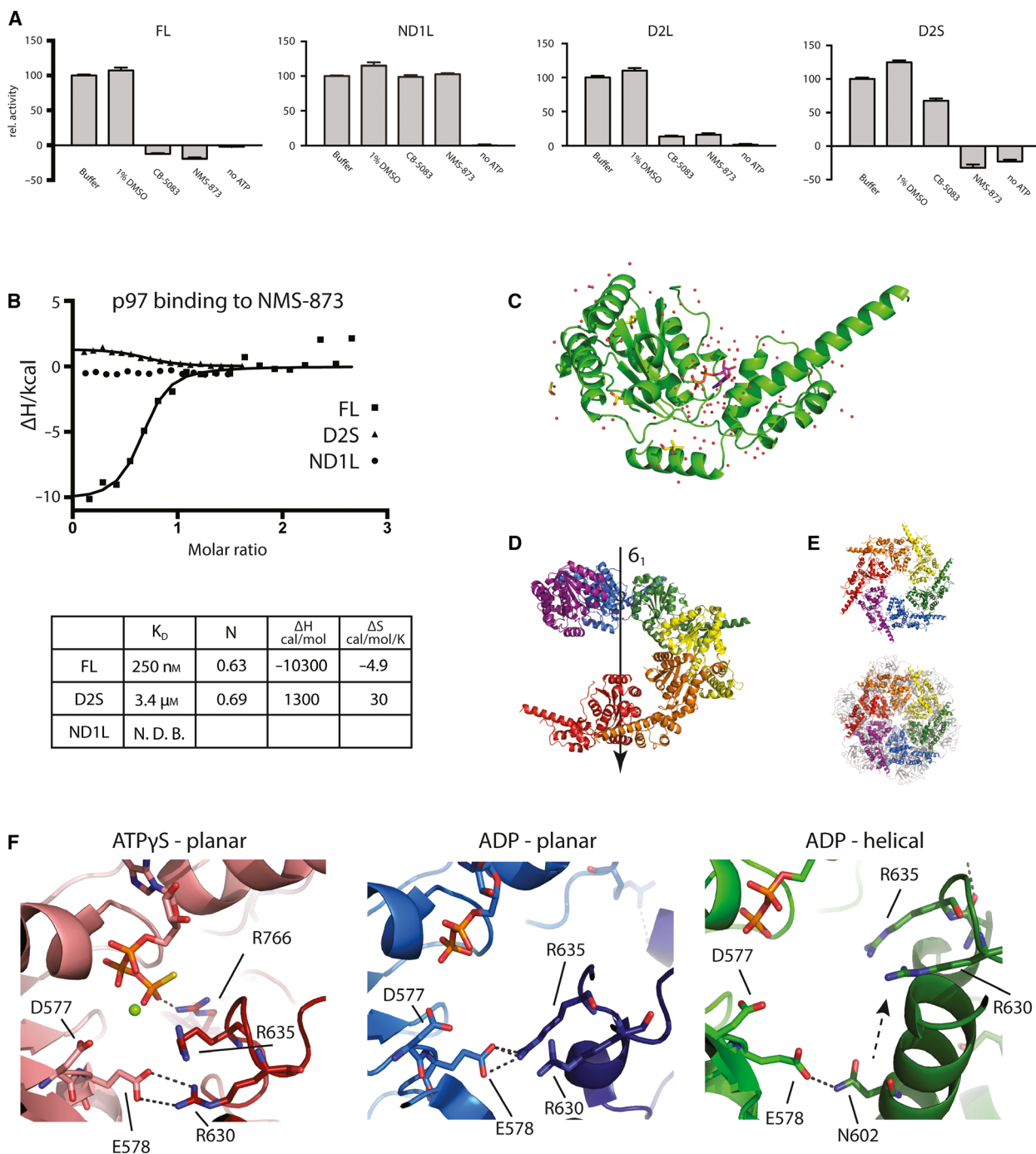


**Fig. 2.** (A) Activity of p97 constructs in the presence of inhibitors, normalised to 100% for buffer only. (B) Binding of NMS-873 to p97 constructs measured by ITC. Table of binding parameters below. (C) Cartoon representation of one p97 D2S domain from crystal structure with water molecules shown as red dots and ligands shown as sticks. ATP in purple and DMSO and MPD in yellow. (D) Cartoon representation of six consecutive D2S domains along the screw axis. (E) Top: Same 6 D2S domains as in D viewed down the screw axis. Bottom: FL p97 (PDB: 5FTK) viewed from 'below' with the D2 domains closest to the observer. (F) Comparison of interprotomer contacts near the ATP binding site. Cartoon representation of planar p97 in the presence of ATP $\gamma$ S (red, PDB: 5FTL), ADP (blue, PDB: 5FTK) and the helical p97 (green). Cartoon representation with key residues and ligands shown as sticks. Magnesium ion shown as green ball.

Strikingly, the crystals with fragments bound diffracted to significantly higher resolution (2.08 and 2.15 Å, respectively) and were the best diffracting crystals of the ones collected. Thus, a manual inspection of all data sets with resolution better than 2.8 Å was carried out and three additional fragments were

identified using this approach. It is possible that crystal-to-crystal variability in unit-cell parameters was the most likely cause why PANDDA could not be used to identify these hits.

All five fragments identified bind in the same groove on the p97 D2 domain (Figs 3 and S2). The fragments

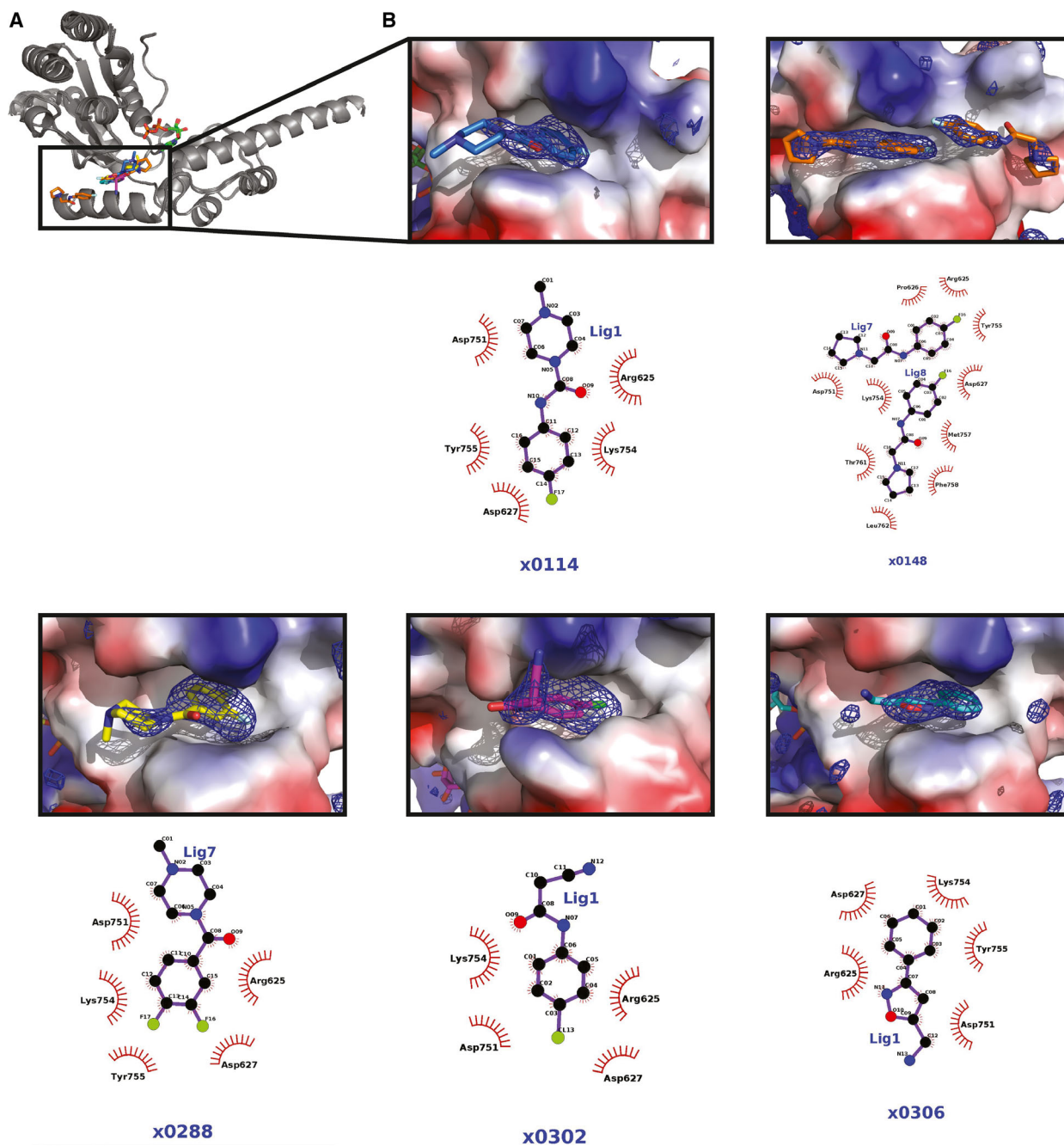


**Fig. 3.** (A) p97 D2S crystal structures of five XChem hits aligned and shown as grey cartoon. ADP shown as sticks in green and XChem hits shown as sticks in same colours as in B. (B) Close-up of interactions of XChem ligands with D2S domain. D2S shown as surface colour according to charge, ligand shown as sticks and polder map shown as mesh in blue contoured at  $3\sigma$ . Chemical structure of ligand shown below with interacting protein residues indicated.

have in common phenyl group that fits into the cavity on the protein surface. In four out of the five hits, these phenyl groups are halogenated, and where organofluorine compounds were identified (114, 148, 302 and 306), the fluorine atoms make extensive contacts (moderate-to-weak electrostatic interactions) with main chain and side chain atoms of surrounding amino acids Asp627, Tyr 755 and Lys 754. Away from the fragment phenyl ring, electrostatic interactions can be seen with neighbouring Arg625, Asp751 and Lys754 side chains. In the case of the structure for p97 bound to compound  $\times 0148$ , two copies of the  $\times 0148$  fragment are present. One copy is bound in a similar conformation in the same site to the other hits identified. The second copy is bound further downstream of the p97 D2 groove ( $\sim 4.5$  Å apart) and interacts with another subset of p97 amino acids. Thr761, Met757 and Phe758 make contacts with the compound's oxygen atom, and the nitrogen atom of the compound's pyrrolidine ring structure hydrogen bonds with the main chain oxygen of Phe758 and the side chain oxygen of Thr761. These observations provide insights on how these potential lead compounds could be extended into the D2 groove.

### Comparison of p97 D2S structure with VAT

The helical parameters of the  $6_1$  screw axis are highly similar to a cryo-EM structure of VAT in a helical

oligomerisation state [26]. It has been observed that around half of VAT molecules are in a split-washer conformation when incubated with ADP. To probe whether the helical arrangement found in our p97 D2S structure is related to the VAT split washer, a model was built where the structures of six FL, ADP-bound, p97 protomers (PDB: 5FTK) were superimposed on six consecutive D2S symmetry mates along the screw axis (Fig. 3A). Strikingly, this theoretical model of p97, based on the D2S crystal symmetry presented here, overlays well with the published cryo-EM map of VAT (rmsd = 36.169) [22]. While no such split-washer particles have been observed in cryo-EM studies of mammalian p97, the high degree of similarity between the VAT structure and the D2S screw axis symmetry suggests that p97 can form a 'split-washer'-type conformation during its ATPase cycle. At the centre of this theoretical model, the D1 of one protomer lines up next to the D2 of its neighbour creating a continuous filament of 12 ATPase domains (Fig. 3A).

### Discussion

p97 is implicated in numerous cellular processes and has been the target of a multitude of biochemical and drug discovery studies [42,4]. Nonetheless, a high-resolution structure of the main catalytic D2 domain, which may aid drug discovery, has been elusive. In

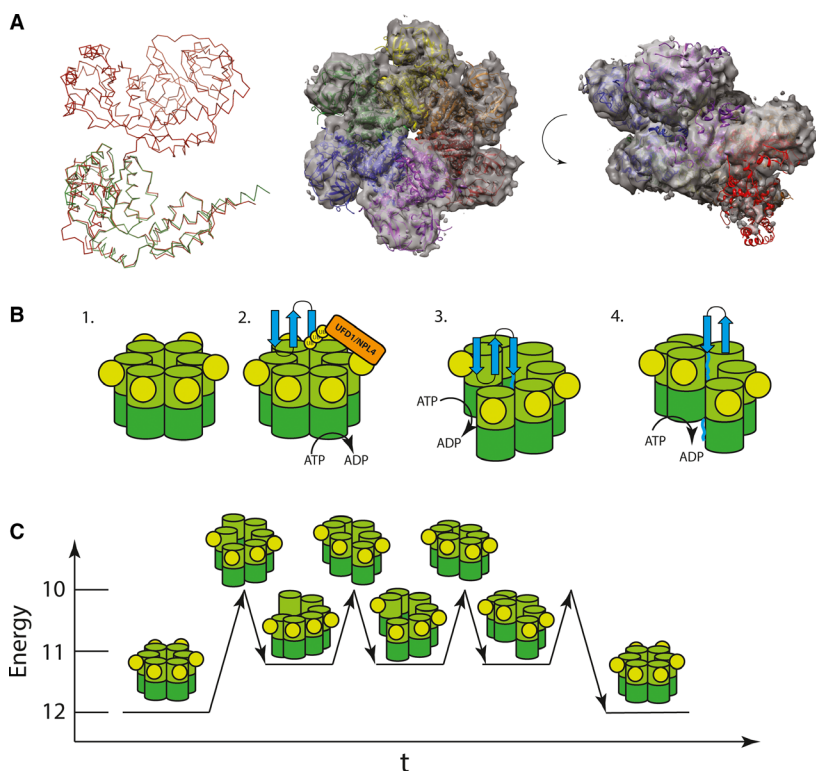


**Fig. 4.** (A) Ribbon representation of one FL p97 protomer (red, PDB: 5FTK) and D2S crystal structure. Structural model of 6 FL p97 protomers arranged along the  $P6_1$  screw axis of the crystal as in Fig. 2D, fitted into the electron density of ADP-bound p97 homologue VAT (EMDB: 3436) shown as transparent surface at contour level 0.0367. (B) Proposed model of p97-mediated substrate unfolding. A substrate (blue) is threaded through the central pore of p97, being progressively unfolded using the consecutive ATP hydrolysis steps. Each ATP hydrolysis step pushes another protomer upwards causing further unfolding. (C) Energy levels of p97 hexamer throughout unfolding process. The planar conformation being the ground state and the filamentous split washer providing a metastable intermediate. Level of interprotomer contacts indicated on y-axis.



addition, the mechanism of force generation required for substrate protein unfolding is not clear. The data presented here provide some steps towards addressing this. The crystal system presented here has been shown to diffract to high resolution, and its solvent channels allow for the soaking of small molecules. The two compounds identified in the XChem screen have a similar chemical group (phenyl moiety) that points into the groove, suggesting that the binding of this class of molecules to D2 is specific. In summary, our XChem experiment has identified a potential hot spot for ligand binding to p97, with five relatively similar fragment hits providing a starting point for the development of more effective p97 allosteric binders that may have p97 inhibitory activity.

In our new D2S high-resolution crystal structure, we observe that the helical parameters of the D2S P<sub>6</sub><sub>1</sub> screw axis are highly similar to the split-washer-type structure determined by cryo-EM for VAT [22] (Fig. 4A). Although speculative, it is possible that the high level of similarity between these two structures is of physiological relevance. If so, then our D2S structure allows us to propose a possible model for force generation for p97, which is not dissimilar to the ratchet-like mechanism reported for Hsp104 [27]. Given that cryo-EM studies have never identified p97 in such a conformation, any split-washer-type species of p97 is likely short-lived and therefore not observable by crystallographic or EM analyses.

Based on this speculation, we can propose a mechanistic model for p97. In its resting state, p97 is in a low-energy planar conformation with twelve inter-ATPase domain contacts. Upon encountering a ubiquitylated substrate *via* adaptor binding, ATP hydrolysis is stimulated as reported by [18]. Hydrolysis in one subunit may cause a conformational change and induce a split-washer conformation by moving one protomer downwards (Fig. 4B). The movement from a planar conformation to a split washer breaks two inter-ATPase domain interactions of  $\sim 1200 \text{ \AA}^2$  in size (Fig. 3E). We propose that this transient conformation is unstable and would likely revert to a more stable planar conformation. However, the twelve-ATPase domain filament provides a metastable intermediate with eleven intradomain interactions (Fig. 4C). This filament may therefore remain stable long enough for another round of ATP hydrolysis, where the next protomer moves downwards, providing a processive mechanism of action that leads to efficient unfolding or target proteins. Hydrophobic interactions between the D2 pore loop and the substrate protein may further stabilise the helical conformation. However, further structural and biophysical work on p97–substrate

complexes would be needed to confirm this speculative p97 mechanistic model.

## Acknowledgements

The expression construct for the ParM ADP-biosensor was kindly provided by Simone Kunzelmann (Francis Crick Institute). We are grateful for the support of the beamline personnel at beamlines I03 and I04-1 at Diamond Light Source with data collection. LS was funded by Cancer Research UK (grant number CRUK A13449). Diamond Light Source hosted and funded the XChem experiment (block allocation group LB-16980).

## Author contributions

LS, XZ and PF devised the study. LS, LM and RM conducted and analysed experiments. AD and FVD provided technology and expertise for the XChem *in crystal* fragment screening. LS, RM and PF wrote and revised manuscript.

## References

- 1 Stach L and Freemont PS (2017) The AAA+ ATPase p97, a cellular multitool. *Biochem J* **474**, 2953–2976.
- 2 Peters JM, Harris JR, Lustig A, Muller S, Engel A, Volker S and Franke WW (1992) Ubiquitous soluble Mg(2+)-ATPase complex. A structural study. *J Mol Biol* **223**, 557–571.
- 3 Peters JM, Walsh MJ and Franke WW (1990) An abundant and ubiquitous homo-oligomeric ring-shaped ATPase particle related to the putative vesicle fusion proteins Sec18p and NSF. *EMBO J* **9**, 1757–1767.
- 4 Meyer H and Weihl CC (2014) The VCP/p97 system at a glance: connecting cellular function to disease pathogenesis. *J Cell Sci* **127**, 3877–3883.
- 5 Kondo H, Rabouille C, Newman R, Levine TP, Pappin D, Freemont P and Warren G (1997) p47 is a cofactor for p97-mediated membrane fusion. *Nature* **388**, 75–78.
- 6 Ye Y, Meyer HH and Rapoport TA (2003) Function of the p97-Ufd1-Npl4 complex in retrotranslocation from the ER to the cytosol: dual recognition of nonubiquitinated polypeptide segments and polyubiquitin chains. *J Cell Biol* **162**, 71–84.
- 7 Dai RM, Chen E, Longo DL, Gorbea CM and Li CC (1998) Involvement of valosin-containing protein, an ATPase Co-purified with IkappaBalpha and 26 S proteasome, in ubiquitin-proteasome-mediated degradation of IkappaBalpha. *J Biol Chem* **273**, 3562–3573.
- 8 Fullbright G, Rycenga HB, Gruber JD and Long DT (2016) p97 promotes a conserved mechanism of helicase

- unloading during DNA cross-link repair. *Mol Cell Biol* **36**, 2983–2994.
- 9 van den Boom J, Wolf M, Weimann L, Schulze N, Li F, Kaschani F, Riemer A, Zierhut C, Kaiser M, Iliakis G *et al.* (2016) VCP/p97 extracts sterically trapped Ku70/80 rings from DNA in double-strand break repair. *Mol Cell* **64**, 189–198.
  - 10 Watts GD, Wymer J, Kovach MJ, Mehta SG, Mumm S, Darvish D, Pestronk A, Whyte MP and Kimonis VE (2004) Inclusion body myopathy associated with Paget disease of bone and frontotemporal dementia is caused by mutant valosin-containing protein. *Nat Genet* **36**, 377–381.
  - 11 Zhou HJ, Wang J, Yao B, Wong S, Djakovic S, Kumar B, Rice J, Valle E, Soriano F, Menon MK *et al.* (2015) Discovery of a first-in-class, potent, selective, and orally bioavailable inhibitor of the p97 AAA ATPase (CB-5083). *J Med Chem* **58**, 9480–9497.
  - 12 Banerjee S, Bartesaghi A, Merk A, Rao P, Bulfer SL, Yan Y, Green N, Mroczkowski B, Neitz RJ, Wipf P *et al.* (2016) 2.3 Å resolution cryo-EM structure of human p97 and mechanism of allosteric inhibition. *Science* **351**, 871–875.
  - 13 Huyton T, Pye VE, Briggs LC, Flynn TC, Beuron F, Kondo H, Ma J, Zhang X and Freemont PS (2003) The crystal structure of murine p97/VCP at 3.6 Å. *J Struct Biol* **144**, 337–348.
  - 14 Rouiller I, Butel VM, Latterich M, Milligan RA and Wilson-Kubalek EM (2000) A major conformational change in p97 AAA ATPase upon ATP binding. *Mol Cell* **6**, 1485–1490.
  - 15 Bodnar NO, Kim KH, Ji Z, Wales TE, Svetlov V, Nudler E, Engen JR, Walz T and Rapoport TA (2018) Structure of the Cdc48 ATPase with its ubiquitin-binding cofactor Ufd1-Npl4. *Nat Struct Mol Biol* **25**, 616–622.
  - 16 Song EJ, Yim SH, Kim E, Kim NS and Lee KJ (2005) Human Fas-associated factor 1, interacting with ubiquitinated proteins and valosin-containing protein, is involved in the ubiquitin-proteasome pathway. *Mol Cell Biol* **25**, 2511–2524.
  - 17 Hanzelmann P and Schindelin H (2017) The interplay of cofactor interactions and post-translational modifications in the regulation of the AAA+ ATPase p97. *Front Mol Biosci* **4**, 21.
  - 18 Blythe EE, Olson KC and Chau V (2017) Deshaies RJ (2017) Ubiquitin- and ATP-dependent unfoldase activity of P97/VCP\*NPLOC4\*UFD1L is enhanced by a mutation that causes multisystem proteinopathy. *Proc Natl Acad Sci USA* **114**, E4380–E4388.
  - 19 Bodnar NO and Rapoport TA (2017) Molecular mechanism of substrate processing by the Cdc48 ATPase complex. *Cell* **169**, 722–735.e729
  - 20 Briggs LC, Baldwin GS, Miyata N, Kondo H, Zhang X and Freemont PS (2008) Analysis of nucleotide binding to P97 reveals the properties of a tandem AAA hexameric ATPase. *J Biol Chem* **283**, 13745–13752.
  - 21 Tang WK and Xia D (2016) Role of the D1-D2 Linker of Human VCP/p97 in the asymmetry and ATPase Activity of the D1-domain. *Sci Rep* **6**, 20037.
  - 22 Huang R, Ripstein ZA, Augustyniak R, Lazniewski M, Ginalski K, Kay LE and Rubinstein JL (2016) Unfolding the mechanism of the AAA+ unfoldase VAT by a combined cryo-EM, solution NMR study. *Proc Natl Acad Sci USA* **113**, E4190–E4199.
  - 23 Holm L (2019) Benchmarking fold detection by DaliLite v.5. *Bioinformatics*, **15**, 5326–5327.
  - 24 Gerega A, Rockel B, Peters J, Tamura T, Baumeister W and Zwickl P (2005) VAT, the thermoplasma homolog of mammalian p97/VCP, is an N domain-regulated protein unfoldase. *J Biol Chem* **280**, 42856–42862.
  - 25 Rothballer A, Tzvetkov N and Zwickl P (2007) Mutations in p97/VCP induce unfolding activity. *FEBS Lett* **581**, 1197–1201.
  - 26 Ripstein ZA, Huang R, Augustyniak R, Kay LE and Rubinstein JL (2017) Structure of a AAA+ unfoldase in the process of unfolding substrate. *eLife* **6**, e25754.
  - 27 Gates SN, Yokom AL, Lin J, Jackrel ME, Rizo AN, Kendersky NM, Buell CE, Sweeny EA, Mack KL, Chuang E *et al.* (2017) Ratchet-like polypeptide translocation mechanism of the AAA+ disaggregase Hsp104. *Science* **357**, 273–279.
  - 28 Anderson DJ, Le Moigne R, Djakovic S, Kumar B, Rice J, Wong S, Wang J, Yao B, Valle E, Kiss von Soly S *et al.* (2015) Targeting the AAA ATPase p97 as an approach to treat cancer through disruption of protein homeostasis. *Cancer Cell* **28**, 653–665.
  - 29 Magnaghi P, D'Alessio R, Valsasina B, Avanzi N, Rizzi S, Asa D, Gasparri F, Cozzi L, Cucchi U, Orrenius C *et al.* (2013) Covalent and allosteric inhibitors of the ATPase VCP/p97 induce cancer cell death. *Nat Chem Biol* **9**, 548–556.
  - 30 Davies JM, Brunger AT and Weis WI (2008) Improved structures of full-length p97, an AAA ATPase: implications for mechanisms of nucleotide-dependent conformational change. *Structure* **16**, 715–726.
  - 31 Hanzelmann P and Schindelin H (2016) Structural basis of ATP hydrolysis and intersubunit signaling in the AAA+ ATPase p97. *Structure* **24**, 127–139.
  - 32 Tang WK, Odzorig T, Jin W and Xia D (2019) Structural basis of p97 inhibition by the site-selective anticancer compound CB-5083. *Mol Pharmacol* **95**, 286.
  - 33 Collins PM, Ng JT, Talon R, Nekrosiute K, Krojer T, Douangamath A, Brandao-Neto J, Wright N, Pearce NM and von Delft F (2017) Gentle, fast and effective crystal soaking by acoustic dispensing. *Acta Crystallogr D Struct Biol* **73**, 246–255.
  - 34 Kabsch W (2010) Xds. *Acta Crystallogr D Biol Crystallogr* **66**, 125–132.

- 35 Adams PD, Grosse-Kunstleve RW, Hung LW, Ioerger TR, McCoy AJ, Moriarty NW, Read RJ, Sacchettini JC, Sauter NK and Terwilliger TC (2002) PHENIX: building new software for automated crystallographic structure determination. *Acta Crystallogr D Biol Crystallogr* **58**, 1948–1954.
- 36 Emsley P, Lohkamp B, Scott WG and Cowtan K (2010) Features and development of Coot. *Acta Crystallogr D Biol Crystallogr* **66**, 486–501.
- 37 Pettersen EF, Goddard TD, Huang CC, Couch GS, Greenblatt DM, Meng EC and Ferrin TE (2004) UCSF Chimera—a visualization system for exploratory research and analysis. *J Comput Chem* **25**, 1605–1612.
- 38 Kunzelmann S and Webb MR (2010) A fluorescent, reagentless biosensor for ADP based on tetramethylrhodamine-labeled ParM. *ACS Chem Biol* **5**, 415–425.
- 39 Chou TF, Bulfer SL, Wehl CC, Li K, Lis LG, Walters MA, Schoenen FJ, Lin HJ, Deshaies RJ and Arkin MR (2014) Specific inhibition of p97/VCP ATPase and kinetic analysis demonstrate interaction between D1 and D2 ATPase domains. *J Mol Biol* **426**, 2886–2899.
- 40 Zhang X and Wigley DB (2008) The ‘glutamate switch’ provides a link between ATPase activity and ligand binding in AAA+ proteins. *Nat Struct Mol Biol* **15**, 1223–1227.
- 41 Pearce NM, Krojer T, Bradley AR, Collins P, Nowak RP, Talon R, Marsden BD, Kelm S, Shi J, Deane CM

- et al.* (2017) A multi-crystal method for extracting obscured crystallographic states from conventionally uninterpretable electron density. *Nat Commun* **8**, 15123.
- 42 Deshaies RJ (2014) Proteotoxic crisis, the ubiquitin-proteasome system, and cancer therapy. *BMC Biol* **12**, 94.

## Supporting information

Additional supporting information may be found online in the Supporting Information section at the end of the article.

**Fig. S1.** (A) Raw ATPase assay data for FL, deltaC, ND1L, D2L, D2S constructs used in this study, as well as ParM Standards ( $n = 3$  technical repeats). (B) Raw activity assay data for FL, ND1L, D2L and D2S constructs.

**Fig. S2** (A) Surface representation in grey of p97 D2S crystal structure with all 5 XChem hits (shown in magenta) superposed in the binding groove. Interacting D2S amino acids are shown in green. (B) Close-up of superposed XChem hits coloured in magenta and their interacting residues in the p97 D2S domain binding groove (coloured in green: N624, R625, D627, D751, K754, M757, F758, T761, L762).

**Table S1.** Crystallographic data collection, model, and refinement statistics.